Catalysis Today 142 (2009) 42–51

Contents lists available at ScienceDirect

Catalysis Today

journal homepage: www.elsevier.com/locate/cattod

# Steam reforming of methane, ethane, propane, butane, and natural gas over a rhodium-based catalyst

Benjamin T. Schädel [a], Matthias Duisberg [b], Olaf Deutschmann [a,*]

[a] Institute for Chemical Technology and Polymer Chemistry, University of Karlsruhe, Engesserstr. 20, 76131 Karlsruhe, Germany
[b] Umicore AG & Co. KG, Rodenbacher Chaussee 4, 63403 Hanau-Wolfgang, Germany

ARTICLE INFO

*Article history:*
Available online 11 February 2009

*Keywords:*
Steam reforming
Detailed mechanism
Rh
Numerical simulation
Hydrogen production
Natural gas

ABSTRACT

Steam reforming of methane, ethane, propane, butane, and a sulfur-free natural gas is studied over a rhodium-based monolithic honeycomb catalyst. The product distribution is analyzed as function of temperature (250–900 °C) and steam-to-carbon ratio (2.2–4) for two honeycomb channel densities (600 and 900 cpsi) and an uncoated monolith by gas chromatography and mass spectroscopy. The reactive flow in the single monolith channel is modeled by a two-dimensional flow field description coupled with detailed reaction mechanisms modeling surface and gas-phase kinetics. Ethane, propane, and butane are converted at much lower temperature than methane, also in natural gas mixtures. An impact of the presence of the higher hydrocarbons on methane conversion in steam reforming of natural gas is found. Steam reforming in the pure gas phase occurs only above 600 °C and the product spectrum differs from that of catalytic conversion.

© 2009 Elsevier B.V. All rights reserved.

## 1. Introduction

Steam reforming of hydrocarbons is an important chemical processes [1–3] providing synthesis gas ($H_2$ and CO), which can subsequently be converted to numerous valuable basic chemicals. The most prominent catalysts for the reforming of natural gas are nickel, which is the conventional catalyst in industry, and rhodium. According to literature, rhodium has been extensively studied as catalyst for steam reforming (SR) of methane [4–11] and propane [12–16], but no study has been found for SR of ethane and only one for SR of butane [17].

Modeling of catalytic SR of natural gas has mainly been based on global kinetic expressions [18–20] and thermodynamic calculations [21]. Even though, a variety of detailed multi-step surface reaction mechanisms have been published over the last years, for instance for modeling partial and total oxidation of hydrocarbons over Pt [22–26], Ni [27–31], and Rh [29–33], there is no mechanism available which covers SR of natural gas, which in fact consist of more than methane.

This article presents an experimental and modeling study on steam reforming of methane, ethane, propane, butane, and natural gas over a rhodium-based catalyst. The final objective of this study is the development of a detailed mechanism including conversion of the higher alkanes present in natural gas and potential gas-phase reactions.

Subsequently experiments using ethane, propane, and butane were performed. In natural gases alkanes higher than butane are only found as traces with concentrations less than 0.04% [34] and were not investigated as their influence is negligible.

## 2. Experimental set-up

In this study steam reforming of the different alkanes is investigated at temperatures ranging from 300 to 1000 °C. The experiments were carried out in a tubular flow reactor schematically depicted in Fig. 1. Distilled water for steam production was kept in a pressure reservoir at 3 bar. The flux of liquid water to the vaporizer was electronically controlled by a Bronkhorst Hi-Tec LiquiFlow. The gas compounds argon, methane, ethane, propane, butane, and natural gas were electronically controlled using mass flow controllers (Bronkhorst Hi-Tec F-201C operated with the control unit Bronkhorst Hi-Tec E-700). All gases were provided by AIR LIQUIDE Deutschland GmbH. Those gases were also fed to the homemade vaporizer, a vessel filled with discarded metal slices, which also serves as mixing chamber for fuel and steam.

The reactor itself is made out of the ceramic material Pythagoras and natural stone. The Pythagoras tube which serves as outer reactor wall is glued with silicon between two flanges. These flanges consist of stainless steel and are held at a temperature of 90 °C using ethyleneglycol pumped by a

* Corresponding author.
*E-mail address:* deutschmann@ict.uni-karlsruhe.de (O. Deutschmann).

0920-5861/$ – see front matter © 2009 Elsevier B.V. All rights reserved.
doi:10.1016/j.cattod.2009.01.008

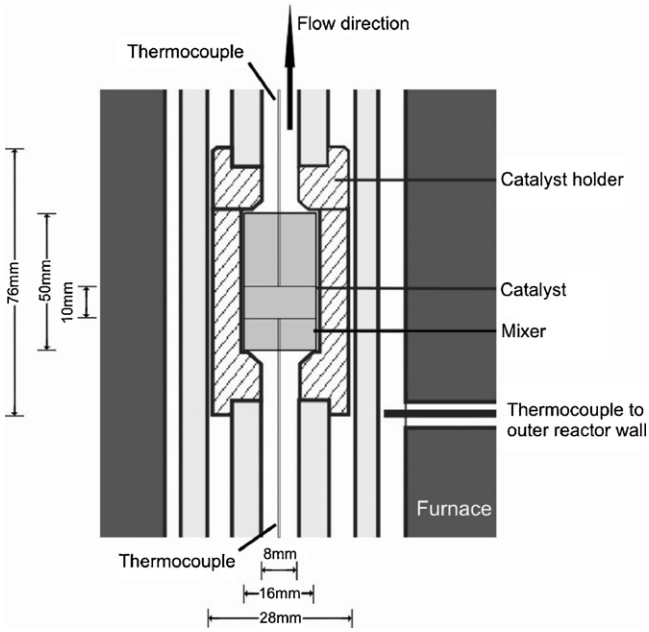


**Fig. 1.** Catalyst holder in the reactor surrounded by the furnace.

thermostat and the heat exchanger MGW Lauda M5. This flange temperature is chosen because it prevents condensation of the water and melting of the silicon glue (melting point ~200 °C). The catalyst inside the reactor is placed in a holder made out of pyrophyllite and is kept at its position using Pythagoras tubes with a smaller diameter. Those tubes have an inner diameter of 8 mm leading to smaller dead volume and faster transport to the catalytic section. The dimensions of the inner tubes ensure reasonably flat temperature profiles at the catalyst entrance.

Monoliths with an overall length of 50 mm and an outer diameter of 1.5 cm can be placed inside the reactor. In the experiments presented here three cordierite monoliths were placed inside. In the upstream position, an uncoated foam monolith with 10 mm in length is placed guaranteeing flat inlet velocity profiles at the entrance of the following catalytically coated honeycomb monolith, also 10 mm in length. Downstream another honeycomb monolith is placed with a length of 30 mm. A ceramic cloth, approximately 1-mm thick, was wound around the monoliths to diminish bypass of gas.

The entire reactor was placed inside a tubular furnace allowing the operation of the reactor at controlled temperatures. The gas temperatures at the front and at the exit of the catalytic monolith are monitored using Rh/Pt-thermocouples type S. The temperature measured at the rear end of the catalyst is chosen as reference temperature in the charts. The temperature of the outer reactor wall measured by a third thermocouple was used to control the power of the furnace. The reactor was operated at slightly higher pressures than atmospheric (1.05 bar).

The product composition was analyzed using a quadrupole mass spectrometer (AIRSENSE 500) and a gas chromatograph (a modified Varian CP-3380 equipped with a Chrompack Silica Plot 8567 and a Chrompack 7514 Fused Silica Carbo Plot P7). The water in the product stream was condensed in a cold trap [35] before entering analysis devices. The mass of the condensed water was determined for every individual experiment at given constant external conditions.

The applied catalyst was provided by Umicore AG & Co. KG Hanau, Germany. In catalyst preparation, alumina slurry containing rhodium as active catalytic component and further additives, which will not be disclosed, were coated on the inner channel walls of the cordierite honeycomb monoliths. Most of this slurry is deposited in the corners of the rectangular shaped channels where the washcoat is up to 150-μm thick. The thickness of the washcoat in the remaining 75% of the channel wall area is between 5 and 25 μm.

Honeycomb monoliths with hydraulic diameters of ~0.9 mm (900 cpsi (channel per square inch)), and 1.3 mm (600 cpsi) were examined. BET-measurements of a catalyst with 900 cpsi lead to a total surface area of 42.97 $m^2/g$, and chemisorption measurements using hydrogen estimate a specific surface area of 0.98 $m^2/g$. The latter value was used to calculate the ratio of the active surface area to the geometrical surface of the channel walls ($F_{cat/geo}$) to be 143. The parameter $F_{cat/geo}$ serves as parameter for the description of the effective catalytic area in the model (Eq. (5)).

In all experiments (Table 2), the gas hourly space velocity (GHSV) was 40,000 $h^{-1}$. The dilution of the feed stream by 75 vol.% argon leads to an effective GHSV of 10,000 $h^{-1}$ for the potentially reactive gases. The dilution helps to preserve isothermal conditions. All measurements were conducted under steady-state conditions. The measuring time of the mass spectrometer at each temperature was 1 h; alternatively, three repetitive measurements were carried out with the GC analysis. The total amount of condensed water during this measurement series for one set of external conditions was analyzed.

## 3. Modeling and simulation approach

In modeling the reactor, the following simplifications have been made:

(1) Since the measured temperature difference between the front and back of the catalyst were always below 10 °C, isothermal conditions can be assumed. The foam monolith in front of the catalyst ensures a uniformly distributed inlet flow at the catalyst front face. Hence, all channels behave essentially alike and only one channel of the monolith needs to be analyzed.
(2) The coating led to almost round channel cross-sections. Therefore, the channel flow can be treated two-dimensional assuming cylindrical coordinates with the axial and radial position as independent variables.
(3) An averaged washcoat thickness of 20 μm was assumed. Along the channel, a uniform distribution of the catalyst can be assumed.
(4) Pressure measurements between the feed section and the vaporizer revealed pressures slightly higher than standard pressure. Since the vaporizer and the foam monolith cause the comparably highest pressure drops, standard pressure is taken as input parameter of the simulations.
(5) The temperature in the combined vaporizer and mixing chamber is 200 °C, which is taken as inlet flow temperature.
(6) The flow in the small channels is laminar indicated by the Reynolds number of approximately $Re = 100$ for 900 cpsi and 700 °C.
(7) Since the Péclet number can be defined as $Pe = Re \cdot Sc$ with the Schmidt number for gases being $Sc \sim 1$, a Péclet number of $Pe \sim 100$ can be calculated for 900 cpsi. Hence, in axial direction, convective transport is more important than diffusive transport and axial diffusion can be neglected [36].

Assumption (7) implies that the flow can be modeled by the so-called boundary-layer equations instead of the full Navier–Stokes equations [36]. Mathematically, the character of the equations is simplified from elliptical to parabolic with a time-like coordinate along the channel axis. These assumptions result in the following

equation system:

$$\frac{\partial(r\rho u)}{\partial z}+\frac{\partial(r\rho v)}{\partial r}=0 \tag{1}$$

$$\frac{\partial(r\rho u Y_i)}{\partial z}+\frac{\partial(r\rho v Y_i)}{\partial r}=-\frac{\partial}{\partial r}(r j_i)+r\dot{\omega}_i \tag{2}$$

$$\frac{\partial(r\rho u u)}{\partial z}+\frac{\partial(r\rho v u)}{\partial r}=-r\frac{\partial p}{\partial z}+\frac{\partial}{\partial r}\left(\mu r\frac{\partial u}{\partial r}\right) \tag{3}$$

$$\frac{\partial(r\rho u h)}{\partial z}+\frac{\partial(r\rho v h)}{\partial r}=ru\frac{\partial p}{\partial z}+\frac{\partial}{\partial r}\left(\lambda r\frac{\partial T}{\partial r}\right)-\frac{\partial}{\partial r}\left(\sum_i r j_i h_i\right) \tag{4}$$

In these equations $\rho$ [kg m$^{-3}$] indicates the mass density of the mixture, $u$ [m s$^{-1}$] the axial and $v$ [m s$^{-1}$] the radial velocity, $r$ [m] the radial and $z$ [m] the axial coordinate, $Y_i$ the mass fraction of species $i$, $\dot{\omega}_i$ [mol m$^{-3}$ s$^{-1}$] the chemical source term due to gas-phase reactions, $j_i$ [kg m$^{-2}$ s$^{-1}$] the diffusive flux, $\mu$ [kg m$^{-1}$ s$^{-1}$] the viscosity, $T$ [K] the temperature, $h_i$ [J kg$^{-1}$] the enthalpy of species $i$, and $\lambda$ [W m$^{-1}$ K$^{-1}$] the thermal conductivity. The transport coefficients ($\mu$, $\lambda$) and the species diffusion fluxes $j_s$ depend on temperature and species composition.

Chemical reactions on the catalytic reactor wall lead to the following boundary condition:

$$j_i+\rho Y_i v_{\mathrm{St}}=\eta F_{\mathrm{cat/geo}}\dot{s}_i M_i \tag{5}$$

Here, $\dot{s}_i$ [mol m$^{-2}$ s$^{-1}$] is the source rate of species $i$ by adsorption and desorption processes, $M_i$ [kg mol$^{-1}$] is the molar mass of species $i$, $j_i$ [kg m$^{-2}$ s$^{-1}$] is the diffusive flux on the surface, $Y_i$ is the mass fraction of species $i$ in the gas phase adjacent to the surface, $v_{\mathrm{St}}$ [m s$^{-1}$] is the Stefan velocity, and $\eta$ is the effectiveness factor for diffusion within the washcoat. In this work, the effectiveness factor was fixed to be $\eta = 1$ due to the thin washcoat layer of approximately 15 μm applied. $F_{\mathrm{cat/geo}}$ is used to model the amount of catalyst exposed to the gas phase and describes the ratio of catalytic to geometric surface area; a value of $F_{\mathrm{cat/geo}} = 143$ as found by chemisorption measurements for the catalyst used in the present study.

The mean field approximation is applied for modeling the surface reactions [37]. This approximation assumes the adsorbed species to be randomly distributed on a uniform surface, described as a function of temperature and coverage that depends only on the macroscopic position on the catalyst. Fluctuations in coverage are averaged on a microscopic scale.

Due to the high temperature, reactions may also occur in the gas phase. Mass transport (molecular diffusion) between the bulk fluid and the walls of the channel then also becomes significant to understand the interaction between surface and gas-phase reactions. The chemical source terms for gas-phase species (Eqs. (8) and (9)) and for the adsorbed species (Eq. (9)) are given by

$$\dot{\omega}_i=\sum_{k=1}^{K_g}\nu_{ik}k_k\prod_{j=1}^{N_g}c_j^{\nu' jk} \quad \text{and} \tag{8}$$

$$\dot{s}_i=\sum_{k=1}^{K_s}\nu_{ik}k_k^{(s)}\prod_{j=1}^{N_g+N_s}\left(c_{sj}^{(s)}\right)^{\nu' jk}, \tag{9}$$

where $K_s$ is the number of surface reactions, $\nu_{ik}$ (product side minus educt side) and $\nu'_{jk}$ (educt side of the reaction equation) are the stoichiometric coefficients, $k_k$, $k_k^{(s)}$ [mol,m,s] are rate coefficient (on the surface), $N_s$ is the number of species on the surface, $N_g$ is the number of species in the gas phase, $c_{sj}$ [mol m$^{-2}$] is the surface concentration, that is the product of surface coverage, $\Theta_i$, and surface site density, $\Gamma$ [37,38]. The surface site density of $\Gamma = 2.77 \times 10^{-9}$ mol/cm$^2$ was estimated for rhodium ($1.67 \times 10^{15}$ atoms/cm$^2$ [39]). Since the experiments were performed under steady-state conditions, Eq. (9) must obey the condition $\dot{s}_i = 0$ for every adsorbed species.

The temperature dependence of the rate coefficients are described by a modified Arrhenius expression:

$$k_k=A_k T^{\beta_k}\exp\left[\frac{-E_{ak}}{RT}\right]\prod_{i=1}^{N_s}\Theta_i^{\mu_{ik}}\exp\left[\frac{\varepsilon_{ik}\Theta_i}{RT}\right], \tag{10}$$

which is extended by an additional factor (product term in Eq. (10)) in case of surface reactions. This extension accounts for the dependence of the rate coefficients on the coverage using the parameters $\mu_{ik}$ and $\varepsilon_{ik}$ [37,38]. The rate coefficient for an adsorption is calculated from initial sticking coefficients $S^0$ by

$$k_i^{(s)}=\frac{S_i^0}{\Gamma^\tau}\sqrt{\frac{RT}{2\pi M_i}}, \tag{11}$$

where $\tau$ is the number of occupied adsorption sites of species $i$.

For the numerical solution of the equation system the computer code DETCHEM$^{\mathrm{CHANNEL}}$ [40,41] was applied. Given the inlet conditions, the boundary-layer equations are solved in a single sweep of integration along the axial direction by a method-of-lines procedure. The radial derivatives are discretized by a finite-volume method. The resulting differential-algebraic equation system is integrated using the semi-implicit extrapolation solver LIMEX [42].

## 4. Reaction mechanisms

### 4.1. Surface reactions

The development of the surface reaction mechanism for steam reforming of natural gas proceeded over several steps. The new mechanism is based on mechanisms previously developed in our group for autothermal reforming (also known as oxidative steam reforming) [43] and partial oxidation [33] of methane over Rh. The autothermal reforming mechanism extends the latter one by introducing four additional reactions of surface-adsorbed HCO. HCO was suggested by Yan et al. [44] to play a crucial role in reforming reactions. The reaction rate constants were calculated by Hei et al. [31] with the UBI-QEP method [45,46].

In this work, further extensions were conducted to enable adequate modeling of steam reforming: aside from minor modifications of rate constants, the reduction of CO(s) by H(s) and the reverse reaction, oxidation of C(s) by OH(s) [31], was included:

$$\mathrm{CO(s)} + \mathrm{H(s)} \rightarrow \mathrm{C(s)} + \mathrm{OH(s)} \quad (A,\ 3.7 \times 10^{21}, \beta,\ 0.0, E_a,\ 142.76) \tag{12}$$

$$\mathrm{C(s)} + \mathrm{OH(s)} \rightarrow \mathrm{CO(s)} + \mathrm{H(s)} \quad (A,\ 3.7 \times 10^{20}, \beta,\ 0.0, E_a,\ 25.54) \tag{13}$$

The mechanism with the associated reaction rate constants is listed in Table 1.

The conversion of each higher alkane is modeled as global step since no theoretical data has been published yet which could be used for elementary steps. Only $C_1$-products were detected during the catalytic experiments, so the addition of further steps is neither possible nor necessary. So adsorption of higher alkanes, $C_{2+}$, is treated in a very simple way by one-step dissociative adsorption yielding carbon and hydrogen atoms on the surface. As rate law of

**Table 1**
Detailed reaction mechanism for steam reforming of methane.

| | Reaction | $A$ (cm, mol, s) | $\beta$ | $E_a$ (kJ mol$^{-1}$) |
|---|---|---|---|---|
| 1. | $H_2 + Rh(s) + Rh(s) \rightarrow H(s) + H(s)$ | $1.000 \times 10^{-02}$[a] | 0.0 | 0.00 |
| 2. | $H(s) + H(s) \rightarrow H_2 + Rh(s) + Rh(s)$ | $3.000 \times 10^{+21}$ | 0.0 | 77.80 |
| 3. | $O_2 + Rh(s) + Rh(s) \rightarrow O(s) + O(s)$ | $1.000 \times 10^{-02}$[a] | 0.0 | 0.00 |
| 4. | $O(s) + O(s) \rightarrow O_2 + Rh(s) + Rh(s)$ | $1.300 \times 10^{+22}$ | 0.0 | 355.20 |
| 5. | $CH_4(s) \rightarrow CH_4 + Rh(s)$ | $8.000 \times 10^{-03}$[a] | 0.0 | 0.00 |
| 6. | $CH_4 + Rh(s) \rightarrow CH_4(s)$ | $2.000 \times 10^{+14}$ | 0.0 | 25.10 |
| 7. | $H_2O + Rh(s) \rightarrow H_2O(s)$ | $1.000 \times 10^{-01}$[a] | 0.0 | 0.00 |
| 8. | $H_2O(s) \rightarrow H_2O + Rh(s)$ | $6.000 \times 10^{+13}$ | 0.0 | 45.00 |
| 9. | $CO_2 + Rh(s) \rightarrow CO_2(s)$ | $1.000 \times 10^{-05}$[a] | 0.0 | 0.00 |
| 10. | $CO_2(s) \rightarrow CO_2 + Rh(s)$ | $3.000 \times 10^{+08}$ | 0.0 | 21.70 |
| 11. | $CO + Rh(s) \rightarrow CO(s)$ | $5.000 \times 10^{-01}$[a] | 0.0 | 0.00 |
| 12. | $CO(s) \rightarrow CO + Rh(s)$ | $1.000 \times 10^{+13}$ | 0.0 | 133.40 |
| | $\theta_{CO(s)}$ | | | 50.0[b] |
| 13. | $H(s) + O(s) \rightarrow OH(s) + Rh(s)$ | $5.000 \times 10^{+22}$ | 0.0 | 83.70 |
| 14. | $OH(s) + Rh(s) \rightarrow H(s) + O(s)$ | $3.000 \times 10^{+20}$ | 0.0 | 37.70 |
| 15. | $H(s) + OH(s) \rightarrow H_2O(s) + Rh(s)$ | $3.000 \times 10^{+20}$ | 0.0 | 33.50 |
| 16. | $H_2O(s) + Rh(s) \rightarrow H(s) + OH(s)$ | $5.000 \times 10^{+22}$ | 0.0 | 110.90 |
| 17. | $OH(s) + OH(s) \rightarrow H_2O(s) + O(s)$ | $3.000 \times 10^{+21}$ | 0.0 | 100.80 |
| 18. | $H_2O(s) + O(s) \rightarrow OH(s) + OH(s)$ | $3.000 \times 10^{+21}$ | 0.0 | 171.80 |
| 19. | $C(s) + O(s) \rightarrow CO(s) + Rh(s)$ | $5.000 \times 10^{+23}$ | 0.0 | 97.90 |
| 20. | $CO(s) + Rh(s) \rightarrow C(s) + O(s)$ | $3.700 \times 10^{+21}$ | 0.0 | 169.00 |
| | $\theta_{CO(s)}$ | | | 50.0[b] |
| 21. | $CO(s) + O(s) \rightarrow CO_2(s) + Rh(s)$ | $1.000 \times 10^{+20}$ | 0.0 | 121.60 |
| | $\theta_{CO(s)}$ | | | 50.0[b] |
| 22. | $CO_2(s) + Rh(s) \rightarrow CO(s) + O(s)$ | $5.000 \times 10^{+21}$ | 0.0 | 115.30 |
| 23. | $CO(s) + H(_s) \rightarrow C(s) + OH(s)$ | $3.700 \times 10^{+21}$ | 0.0 | 142.76 |
| | $\theta_{CO(s)}$ | | | 50.0[b] |
| 24. | $C(s) + OH(s) \rightarrow CO(s) + H(s)$ | $3.700 \times 10^{+20}$ | 0.0 | 25.54 |
| 25. | $CO(s) + H(s) \rightarrow HCO(s) + Rh(s)$ | $5.000 \times 10^{+19}$ | 0.0 | 108.90 |
| 26. | $HCO(s) + Rh(s) \rightarrow CO(s) + H(s)$ | $3.700 \times 10^{+21}$ | 0.0 | 0.00 |
| | $\theta_{CO(s)}$ | | | −50.0[b] |
| 27. | $HCO(s) + Rh(s) \rightarrow CH(s) + O(s)$ | $8.000 \times 10^{+23}$ | 0.0 | 59.50 |
| 28. | $CH(s) + O(s) \rightarrow HCO(s) + Rh(s)$ | $3.700 \times 10^{+21}$ | 0.0 | 167.50 |
| 29. | $CH_4(s) + Rh(3) \rightarrow CH_3(s) + H(s)$ | $5.500 \times 10^{+20}$ | 0.0 | 61.00 |
| 30. | $CH_3(s) + H(s) \rightarrow CH_4(s) + Rh(s)$ | $3.700 \times 10^{+21}$ | 0.0 | 51.00 |
| 31. | $CH_3(s) + Rh(_3) \rightarrow CH_2(s) + H(s)$ | $3.700 \times 10^{+24}$ | 0.0 | 103.00 |
| 32. | $CH_2(s) + H(_s) \rightarrow CH_3(B) + Rh(s)$ | $3.700 \times 10^{+21}$ | 0.0 | 44.00 |
| 33. | $CH_2(s) + Rh(s) \rightarrow CH(s) + H(s)$ | $3.700 \times 10^{+24}$ | 0.0 | 100.00 |
| 34. | $CH(s) + H(s) \rightarrow CH_2(s) + Rh(s)$ | $3.700 \times 10^{+24}$ | 0.0 | 68.00 |
| 35. | $CH(s) + Rh(s) \rightarrow C(s) + H(s)$ | $3.700 \times 10^{+21}$ | 0.0 | 21.00 |
| 36. | $C(s) + H(s) \rightarrow CH(s) + Rh(s)$ | $3.700 \times 10^{+21}$ | 0.0 | 172.80 |
| 37. | $CH_4(s) + O(s) \rightarrow CH_3(s) + OH(s)$ | $1.700 \times 10^{+24}$ | 0.0 | 80.34 |
| 38. | $CH_3(s) + OH(s) \rightarrow CH_4(s) + O(s)$ | $3.700 \times 10^{+21}$ | 0.0 | 24.27 |
| 39. | $CH_3(s) + O(s) \rightarrow CH_2(s) + OH(s)$ | $3.700 \times 10^{+24}$ | 0.0 | 120.31 |
| 40. | $CH_2(s) + OH(s) \rightarrow CH_3(s) + O(s)$ | $3.700 \times 10^{+21}$ | 0.0 | 15.06 |
| 41. | $CH_2(s) + O(s) \rightarrow CH(s) + OH(s)_1$ | $3.700 \times 10^{+24}$ | 0.0 | 114.50 |
| 42. | $CH(s) + OH(s) \rightarrow CH_2(s) + O(s)$ | $3.700 \times 10^{+21}$ | 0.0 | 36.82 |
| 43. | $CH(s) + O(s) \rightarrow C(s) + OH(s)$ | $3.700 \times 10^{+21}$ | 0.0 | 30.13 |
| 44. | $C(s) + OH(s) \rightarrow CH(s) + O(s)$ | $3.700 \times 10^{+21}$ | 0.0 | 136.00 |

Arrhenius parameters for the rate constant written in the form; $k = AT^{\beta} \exp(-E_a/RT)$. Total surface site density is $\Gamma = 2.77 \times 10^{-9}$ mol/cm$^2$.
[a] Sticking coefficient.
[b] Coverage dependent activation energy.

the adsorption of ethane, propane, and butane Eq. (14) was used.

$$\dot{s}_{C_xH_y} = A_k \cdot T^{\beta} \cdot \exp\left(-\frac{E_a}{RT}\right) \cdot c^{a}_{C_xH_y} \cdot c^{b}_{vacancy} \quad (14)$$

The activation energy and the reaction orders, $a$ and $b$, are given in Table 3. We observed a similar behavior in steam reforming of the single components ethane, propane, and butane (for instance, Figs. 4, 5 and 13), consequently, the rate constants lie in a narrow range. The pre-exponential factor is calculated using Eq. (11) [23] assuming a sticking probability of $S_i^0 = 0.006$. The activation energy is expected to be in the order of 50 kJ/mole corresponding to the activation energy for the removal of the first hydrogen atom [30] and is considered to be similar for all alkanes. $\beta = 0$ since no additional temperature dependency is expected. Butane conversion is a bit lower (Figs. 8 and 14). The final value of the parameters were obtained through comparison of experimentally derived and numerically predicted conversion and selectivity in SR of the single components. The adsorbates then participate in the detailed mechanism of the $C_1$-chemistry, Table 1.

**Table 2**
Experimental conditions ($p$ = 1–1.05 bar).

| Feed | T [°C] | S/C | Catalyst (cpsi) |
|---|---|---|---|
| Methane | 460–840 | 2.2 | Rh/umicore (600) |
| Methane | 450–835 | 2.8 | Rh/umicore (600) |
| Methane | 520–845 | 3.3 | Rh/umicore (600) |
| Methane | 425–610 | 3.5 | Rh/umicore (600) |
| Methane | 445–695 | 3.6 | Rh/umicore (600) |
| Methane | 425–845 | 4 | Rh/umicore (600) |
| Methane | 420–820 | 2.7 | Rh/umicore (900) |
| Methane | 420–770 | 3.3 | Rh/umicore (900) |
| Methane | 415–705 | 3.5 | Rh/umicore (900) |
| Methane | 425-950 | 3.8 | Unloaded (600) |
| Ethane | 345–900 | 2.5 | Rh/umicore (900) |
| Ethane | 275–760 | 4 | Rh/umicore (900) |
| Ethane | 540–910 | 2.5 | Unloaded (600) |
| Propane | 335–750 | 2.5 | Rh/umicore (900) |
| Propane | 270–780 | 4 | Rh/umicore (900) |
| Propane | 680–1015 | 4 | Unloaded (600) |
| Butane | 420–720 | 2.5 | Rh/umicore (900) |
| Butane | 320–825 | 4 | Rh/umicore (900) |
| Butane | 540–960 | 4 | Unloaded (600) |
| Natural gas | 240–750 | 2.5 | Rh/umicore (900) |
| Natural gas | 250–750 | 4 | Rh/umicore (900) |
| Natural gas | 540–820 | 2.5 | Unloaded (600) |

### 4.2. Gas-phase reactions

The reactions in the gas phase are included in the simulations applying the mechanism of Quiceno et al. [22]. This mechanism has been developed for oxidation processes of methane, ethane, propane and butane. It consists of 765 reactions among 63 species in the gas phase.

## 5. Results

The steam-to-carbon ratio (S/C), which is the total number of water molecules divided by the total number of carbon atoms in the feed gas, serves as parameter to describe the feed composition. For propane, for example, S/C 3 means 9 molecules of water per molecule propane. For natural gas, an average carbon content per molecule was calculated based on the gas composition. The S/C calculation also accounts for the amount of $CO_2$ contained in the natural gas.

Conversion, selectivity and yield are calculated as follows:

$$X_i = \frac{y_{i,0} - y_{i,e}}{y_{i,0}} \quad (15)$$

$$S_{CO} = \frac{x_{CO}}{x_{CO} + x_{CO_2} + x_{CH_4}}, \quad S_{CO_2} = \frac{x_{CO_2}}{x_{CO} + x_{CO_2} + x_{CH_4}}, \quad S_{CH_4} = \frac{x_{CH_4}}{x_{CO} + x_{CO_2} + x_{CH_4}} \quad (16)$$

$$S_{H_2} = \frac{x_{H_2}}{x_{H_2} + 2 \cdot x_{CH_4}} \quad (17)$$

$$P_p = X_i \cdot S_p \quad (18)$$

**Table 3**
Rate constants for the decomposition of ethane, propane and butane.

| | $E_a$ | $a$ | $b$ |
|---|---|---|---|
| $C_2H_6$ | 51 | 0.6 | 0.87 |
| $C_3H_8$ | 50 | 0.63 | 0.85 |
| $C_4H_{10}$ | 49 | 0.495 | 0.94 |

$\dot{s}_{C_xH_y} = A_k \cdot T^{\beta} \cdot \exp\left(-\frac{E_a}{RT}\right) \cdot c^{a}_{C_xH_y} \cdot c^{b}_{vacancy}$.

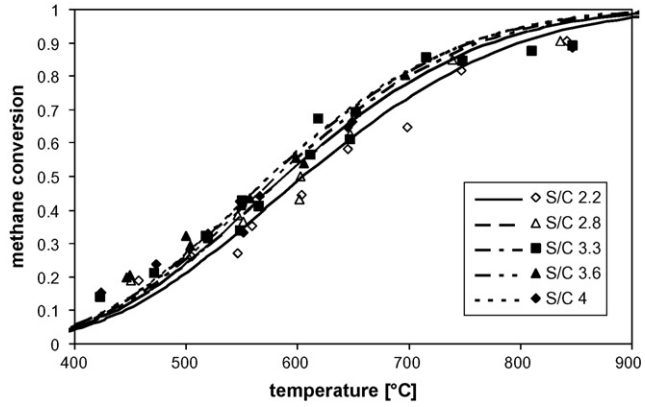


**Fig. 2.** Methane conversion as function of temperature for varying S/C in SR of methane (catalyst with 600 cpsi); symbols: experiment; lines: model predictions.

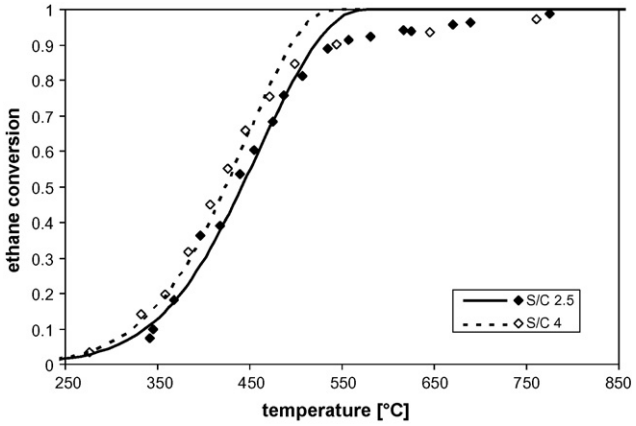


**Fig. 4.** Ethane conversion as function of temperature for varying S/C in SR of ethane (catalyst with 900 cpsi); symbols: experiment; lines: model predictions.

In the equations $X_i$ is the conversion of species $i$, $S_p$ the selectivity of product $p$ ($CH_4$ is product in SR of higher alkanes and natural gas), $P_p$ the yield of product $p$, $y_i$ the mass fraction and $x_i$ the mole fraction of species $i$ in the product stream.

### 5.1. Methane feed

The experiments using methane and water as feed cover a temperature range of 400–850 °C, six S/C ratios ranging from 2.2 to 4 were studied on a catalyst with 600 cpsi. The conversion increases with increasing S/C (Fig. 2). 50% of methane is converted at 600 and 630 °C for S/C 4 and 2.2, respectively. At low temperatures up to 450 °C no CO is produced, all methane converted is totally oxidized to $CO_2$. With increasing temperatures the CO selectivity increases to 63.4% and 46.5% at 845 °C for S/C 2.2 and 4, respectively (Fig. 3).

### 5.2. Ethane feed

For the experiments using the higher alkanes and natural gas as feed stock only two S/C ratios (2.5 and 4) have been examined. For SR of ethane, conversion starts at temperatures exceeding 250 °C (Fig. 4). Conversion above 90% is achieved for temperatures above 550 °C. In case of S/C 2.5, the temperature at which a given conversion is observed is approximately 25 °C lower than in case of S/C 4. CO is the main product at high temperatures (S/C 4 above 900 °C, S/C 2.5 above 700 °C), for both S/C's the selectivity for the formation of $CO_2$ reaches a maximum at about 580 °C, while methane is only produced at low temperatures (40% selectivity at 450 °C).

### 5.3. Propane feed

As in SR of ethane, conversion of propane occurs at temperatures exceeding 250 °C, and the conversion exceeds 90% at temperatures above 500 °C (Fig. 5). Like in SR of ethane the conversion at S/C 4 occurs at 25 °C lower temperatures than in case of S/C 2.5. The selectivity for the formation of methane (up to 40%) exhibits a maximum at temperatures between 400 and 500 °C (Fig. 6). $CO_2$ has a local minimum in this temperature range (selectivity of 44.8% and 55.4% for S/C 2.5 and 4, respectively) and reaches a maximum of 69% selectivity at ~600 °C. At higher temperatures, its selectivity decreases again Products of dehydrogenation reactions or coupling reactions were only observed in traces at temperatures above 800 °C.

### 5.4. Butane feed

The experimental data for SR of butane show that conversion starts at 300 °C and is complete for temperatures exceeding 600 °C conversion (Fig. 7). The conversion at S/C 2.5 equals the conversion at S/C 4 for 30 °C lower temperature. The behavior of selectivity is similar SR of ethane and propane.

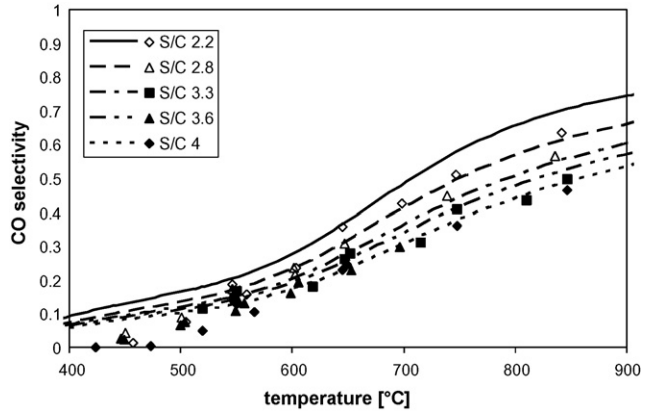


**Fig. 3.** CO selectivity as function of temperature for varying S/C in SR of methane (catalyst with 600 cpsi); symbols: experiment; lines: model predictions.

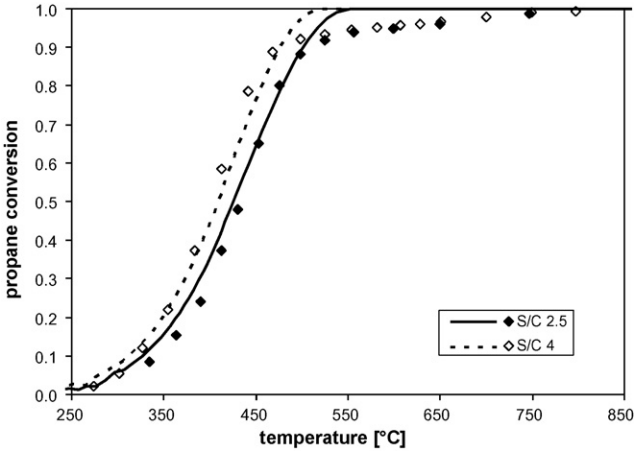


**Fig. 5.** Propane conversion as function of temperature for varying S/C in SR of propane (catalyst with 900 cpsi); symbols: experiment; lines: model predictions.

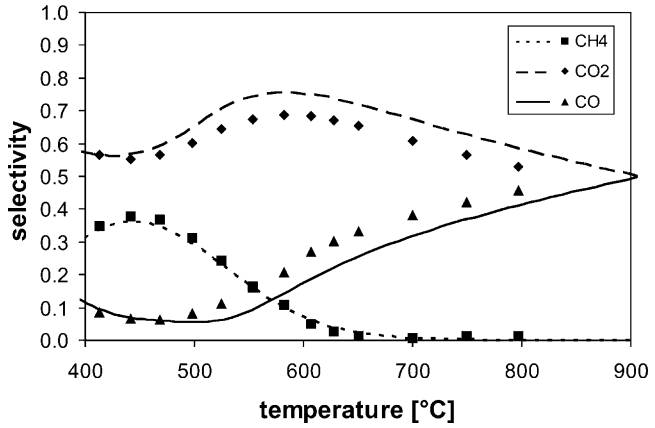


**Fig. 6.** Methane (■), CO (▲), and $CO_2$ (◆) selectivity as function of temperature for S/C 4 in SR of propane (catalyst with 900 cpsi); symbols: experiment; lines: model predictions.

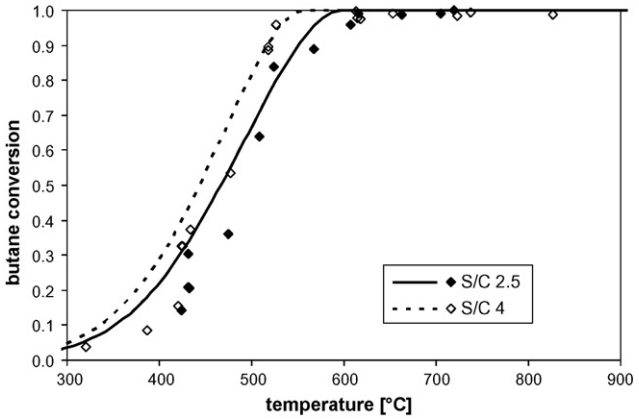


**Fig. 7.** Butane conversion as function of temperature for varying S/C in SR of butane (catalyst with 900 cpsi); symbols: experiment; lines: model predictions.

### 5.5. Natural gas (Nordsee H) feed

The composition of the sulfur-free natural gas (Nordsee H) used in this study is given in Table 4. Steam reforming at S/C ratios of 2.5 and 4 was studied. The conversion of alkanes occurs in two temperature ranges: at temperatures below 400 °C for S/C 4 (450 °C for S/C 2.5) ethane, propane, and butane are almost completely converted (Figs. 8 and 9). Conversion of methane is not observed before the conversion of the higher alkanes is nearly complete. Fig. 10 shows the selectivity for SR of natural gas: methane production is only observed at temperatures below 450 °C with a maximum around 400 °C, $CO_2$ selectivity rises to nearly 100% at 450 °C and diminishes at higher temperatures where an increasing amount of CO is produced.

**Table 4**
Composition of natural gas North Sea H.

| | vol.% |
|---|---|
| $CO_2$ | 1.87 |
| $N_2$ | 0.94 |
| $O_2$ | <0.01 |
| $CH_4$ | 86.72 |
| $C_2H_6$ | 8.10 |
| $C_3H_8$ | 2.03 |
| $C_4H_{10}$ | 0.44 |
| $C_5H_{12}$ | 0.07 |
| $>C_5$ | 0.03 |

Taken from Ruhrgas [34].

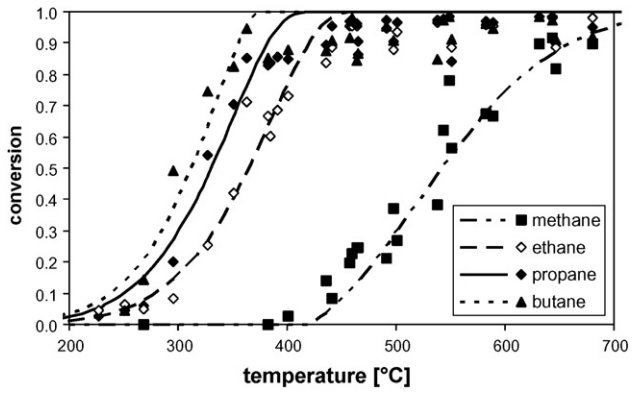


**Fig. 8.** Methane (■), ethane (◇), propane (◆), and butane (▲) conversion as function of temperature for S/C 4 in SR of natural gas (catalyst with 900 cpsi); symbols: experiment; lines: model predictions.

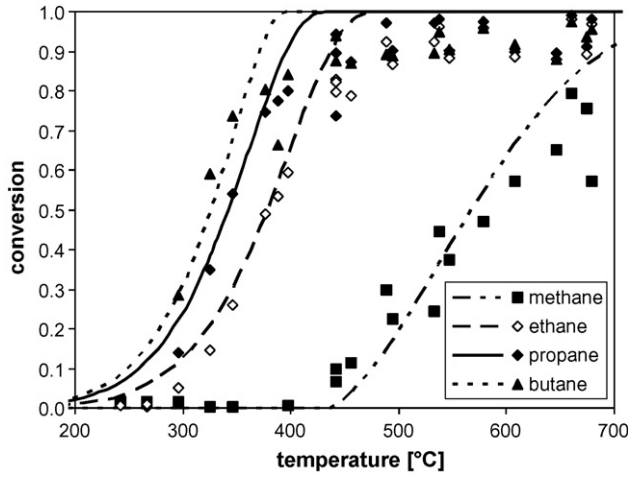


**Fig. 9.** Methane (■), ethane (◇), propane (◆), and butane (▲) conversion as function of temperature for S/C 2.5 in SR of natural gas (catalyst with 900 cpsi); symbols: experiment; lines: model predictions.

### 5.6. Conversion in the gas phase

To investigate the significance of gas-phase reactions, experiments with an uncoated honeycomb monolith have been performed. Methane is not converted up to temperatures of 950 °C. Ethane, propane, and butane are converted above 650 °C

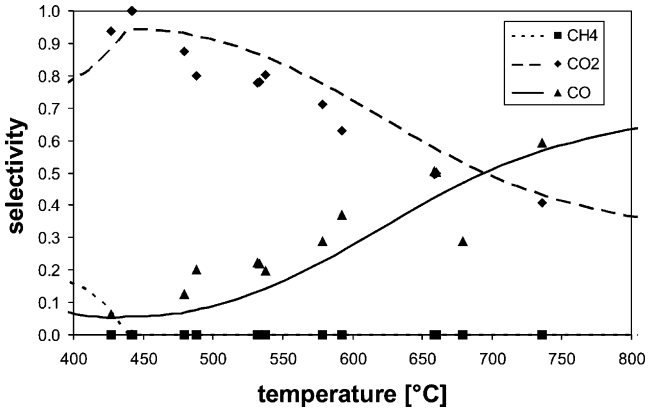


**Fig. 10.** Methane (■), CO (▲), and $CO_2$ (◆) selectivity as function of temperature for S/C 2.5 SR of natural gas (catalyst with 900 cpsi); symbols: experiment; lines: model predictions.

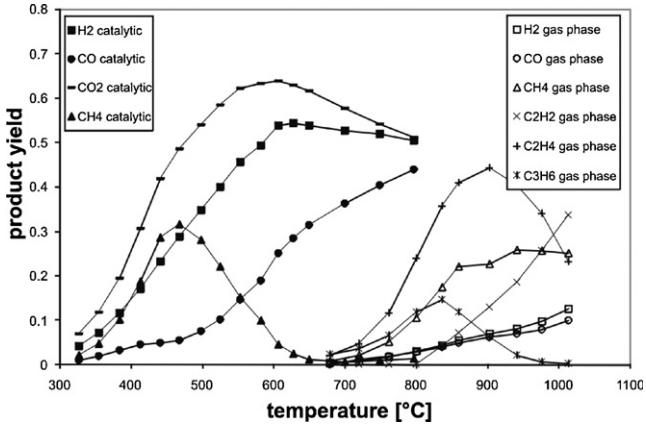


**Fig. 11.** Experimentally determined product yields in catalytic (catalyst with 900 cpsi) and homogeneous SR of propane with S/C 4; filled symbols: with catalyst; open symbols: without catalyst.

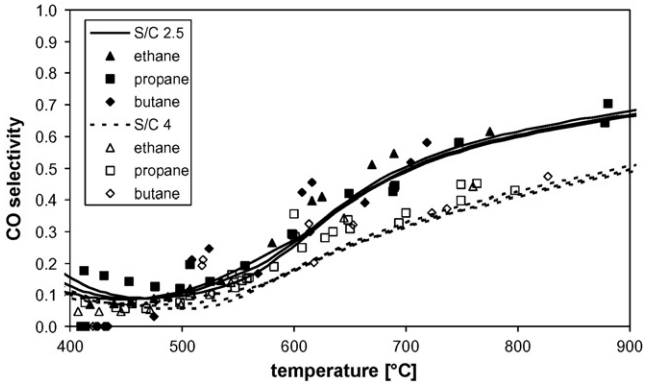


**Fig. 13.** CO selectivity in SR of ethane (▲), propane (■), and butane (◆); filled symbols/full lines: S/C 2.5, open symbols/dashed lines: S/C 4; symbols: experiment, lines: simulation.

and complete conversion is reached at 900 °C. Water is only converted to a minor extend (below 5%). The product spectrum differs significantly from those of the catalytic experiments and are dominated by unsaturated hydrocarbons.

The influence of S/C is negligible due to the low water conversion. Although it would be more appropriate to call this process hydrocracking instead of steam reforming due to the low water conversion, the latter notation will still be used further on for continuity.

Only some experiments with one S/Cs per alkane and few temperatures are carried out in order to test the suitability of the chosen gas-phase mechanism. In non-catalytic SR of ethane with S/C 2.5 at 920 °C, the selectivities of the three major carbon-containing products are 50.3% $C_2H_4$, 29.0% $C_2H_2$, and 10.7% $CH_4$. In SR of propane with S/C 4 at 940 °C we found 41.2% $C_2H_4$, 26.4% $CH_4$, and 19.0% $C_2H_2$, and in SR of butane with S/C 4 at 840 °C 55.7% $C_2H_4$, 15.3% $CH_4$, and 11.7% $C_3H_6$. Fig. 11 shows as example propane conversion and the yield of the main products of SR of propane with S/C 4 with and without catalyst.

## 6. Discussion

Conversion (Figs. 2, 4, 5 and 7–9) and product selectivity (Figs. 3, 6 and 13) in steam reforming of alkanes depend on S/C. The conversion of all alkanes slightly increases with increasing S/C for a given temperature. The decreasing increments of conversion with more steam addition (Fig. 2) is caused by the thermodynamics of the system (Fig. 12). CO selectivity strongly increases with rising temperature but falls with rising S/C (Figs. 3 and 13) according to the water-gas shift equilibrium:

$$H_2O + CO \rightarrow CO_2 + H_2. \quad (19)$$

There is little difference between ethane, propane, and butane concerning the CO selectivity as function of temperature and S/C (Fig. 13); CO selectivity actually shows a minimum at low temperatures, where methane selectivity peaks (Fig. 6). All alkanes show higher CO selectivity for lower S/C again. Both the simulation and experiment indicate no significant differences between conversion and selectivity of the individual $C_2$–$C_4$ alkanes (Fig. 14).

The temperature dependence of the selectivity is dominated by CO at high temperatures and $CO_2$ at low and mediocre temperatures; methane is only formed at low temperatures agreeing with the thermodynamic trends (Fig. 15). The selectivity of SR of the higher alkanes is close to the values at thermodynamic equilibrium except at temperature below 400 °C, where methane is the thermodynamically favored product. The selectivity of CO in steam reforming of methane is lower than the thermodynamic limit due to surface kinetics.

As expected, the conversion of methane increases with increasing surface to volume ratio, whereas no significant influence of the cross-section of the individual channels on selectivity is observed (Figs. 4 and 5). A catalyst with 900 cpsi (channels per square inch) leads to higher conversion of methane (Fig. 16) and, for temperatures exceeding 570 °C, a slightly higher CO selectivity than a 600 cpsi catalyst.

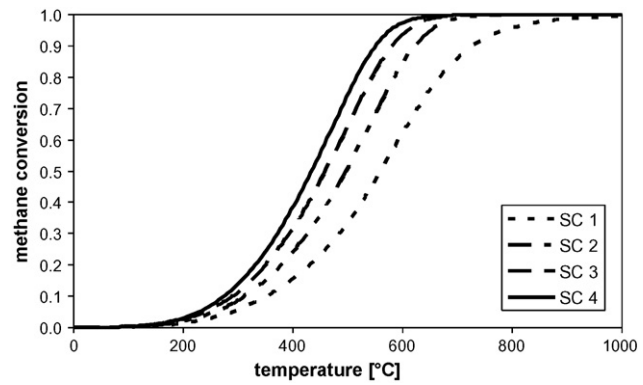


**Fig. 12.** Methane conversion at thermodynamic equilibrium as function of temperature for methane/steam mixtures with varying S/C.

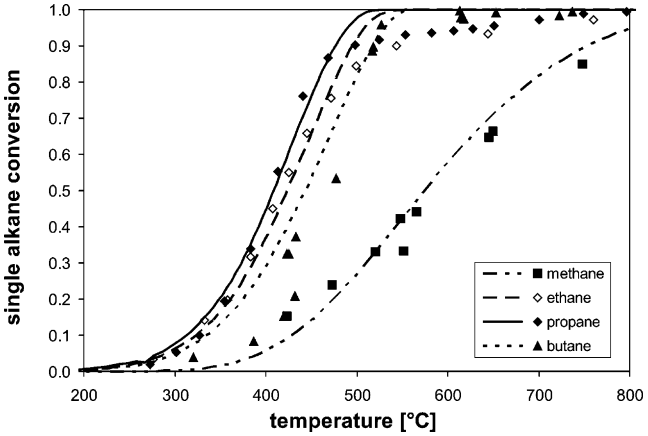


**Fig. 14.** Conversion of methane (■), ethane (◇), propane (◆), and butane (▲) in SR of the individual alkanes. S/C = 4; symbols: experiment, lines: simulation.

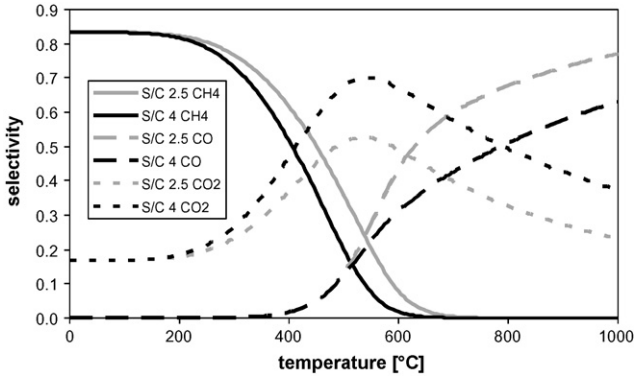


**Fig. 15.** Product selectivity at thermodynamic equilibrium in SR of propane.

At temperatures below 400 °C, SR of natural gas leads to a net methane production (Fig. 10). Since methane is little converted in this temperature range (Fig. 2), the selectivity is mostly determined by the higher alkanes. Compared with SR of methane as single component gas, the net conversion of methane starts at higher temperatures but increases faster with increasing temperature (Fig. 17). Below 400 °C, methane is faster formed from higher hydrocarbons than decomposed, because it is not very reactive at those low temperatures. Since, the higher hydrocarbons are converted first leading also to increased methane concentration, the S/C ratio decreases for methane and increases for the higher alkanes. Therefore, the higher hydrocarbons are not only reformed with S/C = 4 but with S/C ~7 in this temperature range. The conversion of the higher alkanes at temperatures above 450 °C is high for all S/C ratios. If one considers a minimum amount of steam for the conversion of the higher alkanes, e.g. S/C = 1, the remaining steam would increase the S/C for methane from 4 to 4.8 leading to a higher conversion compared to steam reforming of methane. The lower methane conversion in steam reforming of natural gas between 400 and 450 °C is a result of the net methane production due to the high conversion of the higher alkanes and a possibly low methane conversion.

Alkanes higher than methane are likely to react not only on the catalytic surface, but also in the gas phase. The comparison of the experimentally observed behavior of the reactor with and without catalytic coating of the monoliths (Fig. 11) reveals that alkane conversion occurs at considerably higher temperature without catalyst. The product spectrum of purely homogeneous conversion (no catalytic coating) leads to unsaturated hydrocarbons (ethylene, acetylene, propylene; composition depends on fuel, temperature, and S/C). These products could barely be found in the presence of a catalyst. Consequently, the catalyst is either not selective for them or gas-phase intermediates are adsorbed and consumed on the

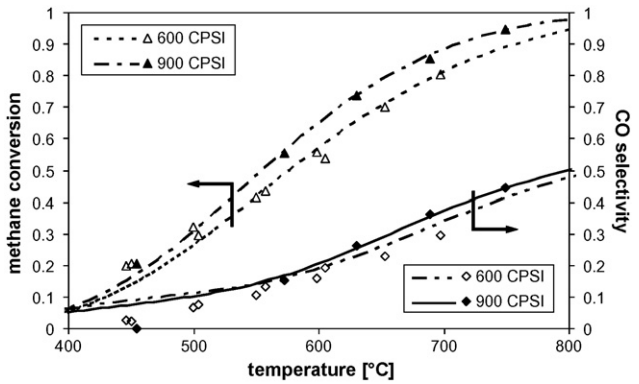


**Fig. 16.** Impact of channel density on methane conversion and CO selectivity in SR of methane with S/C 3.3; symbols: experiment, lines: simulation.

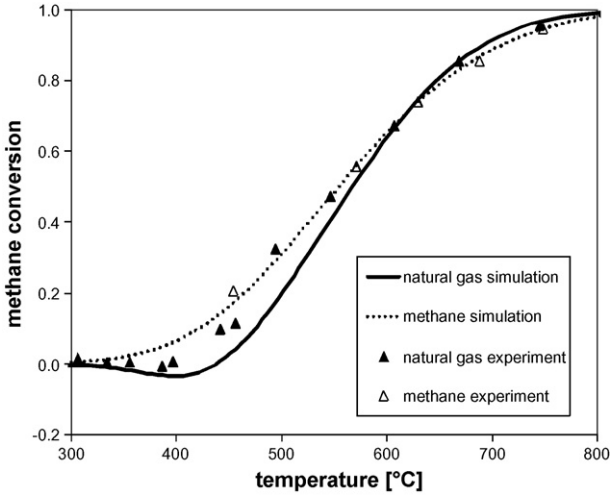


**Fig. 17.** Comparison of experimentally derived methane conversion in SR of natural gas (▲) and SR of methane (△); cpsi 900, S/C 2.5.

catalyst. The product distribution of the non-catalytic conversion experiments are well-predicted by the numerical simulation. The analysis of the simulation results for the catalytic system, as discussed below, reveals that at the high temperatures, at which SR by gas-phase reactions occurs, the higher alkanes are totally converted in the first region of the catalyst. Therefore, there is not enough time (length) to build-up a radical pool in the gas phase to initiate significant conversion in the gas phase, which means, the ignition delay time is larger than the lifetime of the higher alkanes in the catalyst. Actually, to fully understand the interaction between gas phase and surface reactions one needs to include adsorption and desorption of radicals in the surface reaction mechanism. However, as the results and discussion above shows these steps are not significant for the catalyst considered here.

The yield of hydrogen depends on temperature and S/C. The yield can either be calculated for the conversion of the alkane or the conversion of alkane and water. Fig. 18 presents the yield based on the alkane conversion only. The hydrogen yield increases with increasing S/C and increasing chain-length of the alkanes. Only propane is shown as example for the higher alkanes in Fig. 18 since their curves lie closely together. The hydrogen is produced either from the steam reforming reaction or the water-gas shift. The first one remains constant as soon as full conversion is reached. The decline of the water-gas shift, indicated by the increasing

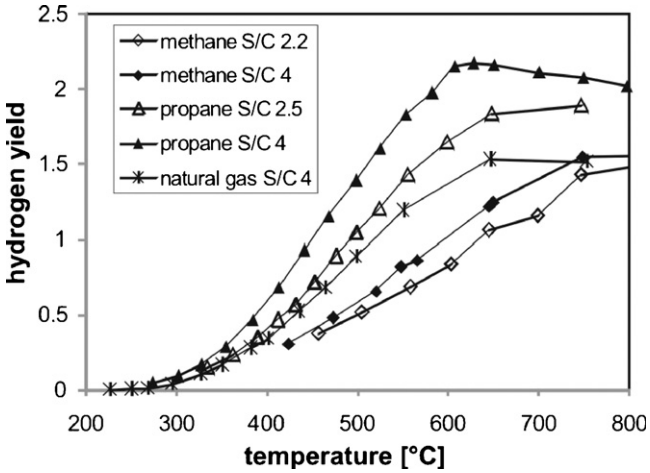


**Fig. 18.** Comparison of experimentally determined hydrogen yields in SR of methane with S/C 2.5 (◇) and S/C 4 (◆), steam reforming of natural gas with S/C 4 (*), steam reforming of propane with S/C 2.5 (△) and S/C 4 (▲).

selectivity of CO, with increasing temperatures leads to a decline of the overall hydrogen production. The slope for the higher alkanes is steeper than for methane and their yields for a given S/C are closer together. The curve for the hydrogen yield from natural gas follows below 450 °C the curves of the higher alkane propane and approaches the yield from SR of methane as soon as methane in the natural gas is converted.

Fig. 19 shows the numerically predicted spatial distribution of the species in the gas phase inside the catalytic channel for SR of natural gas with S/C 4. At 327 °C (Fig. 19a) no conversion of methane and only low to moderate conversion of the higher alkanes is observed, nearly all carbon is converted to CO. Low conversion of methane is found at 452 °C (Fig. 19b), while the higher alkanes are already completely converted at this temperature. The rapidly produced CO is re-adsorbed and further reacts to $CO_2$ via the water-gas shift reaction (19). Further discussion on that issue can be found in our recent paper [47]. At 577 °C (Fig. 19c) the conversion of all reactants is nearly complete. $CO_2$ is still the main product, but since the influence of the slightly exothermic water-gas shift reaction declines with increasing temperatures, CO is increasingly found in the product stream. A comparison of all temperatures reveals that the reaction zone is moving to the front of the catalyst with increasing temperatures.

Fig. 20 shows the calculated temperature dependence of the surface coverage in SR of natural gas with S/C 4. At high temperatures, the surface is mostly empty denoted by the vacant sites Rh(s). Molecular hydrogen is available on the surface in the percent range with a maximum coverage of 6.8% at 390 °C and declines with increasing temperatures to 0.8% at 1000 °C. The primarily found species is CO(s) (Fig. 20). At first view, this result produced in terms of the reaction kinetics developed in this study seems to be contradictory to literature [48] claiming the CO coverage to be negligible at elevated temperatures. Other authors [39,49,50] observed in temperature programmed desorption (TPD) experiments a high coverage of CO at low temperatures and desorption temperatures of CO between 182 and 267 °C depending on surface type and experimental set-up. The coverage of CO in our simulation decreases with increasing temperature, from 76% at 200 °C to 2.5% at 1000 °C, which still is a significantly high value and definitely larger than one may expected. This apparent inconsistency can easily be resolved: the very active Rh catalyst is exposed to a hydrocarbon stream that continuously produces new

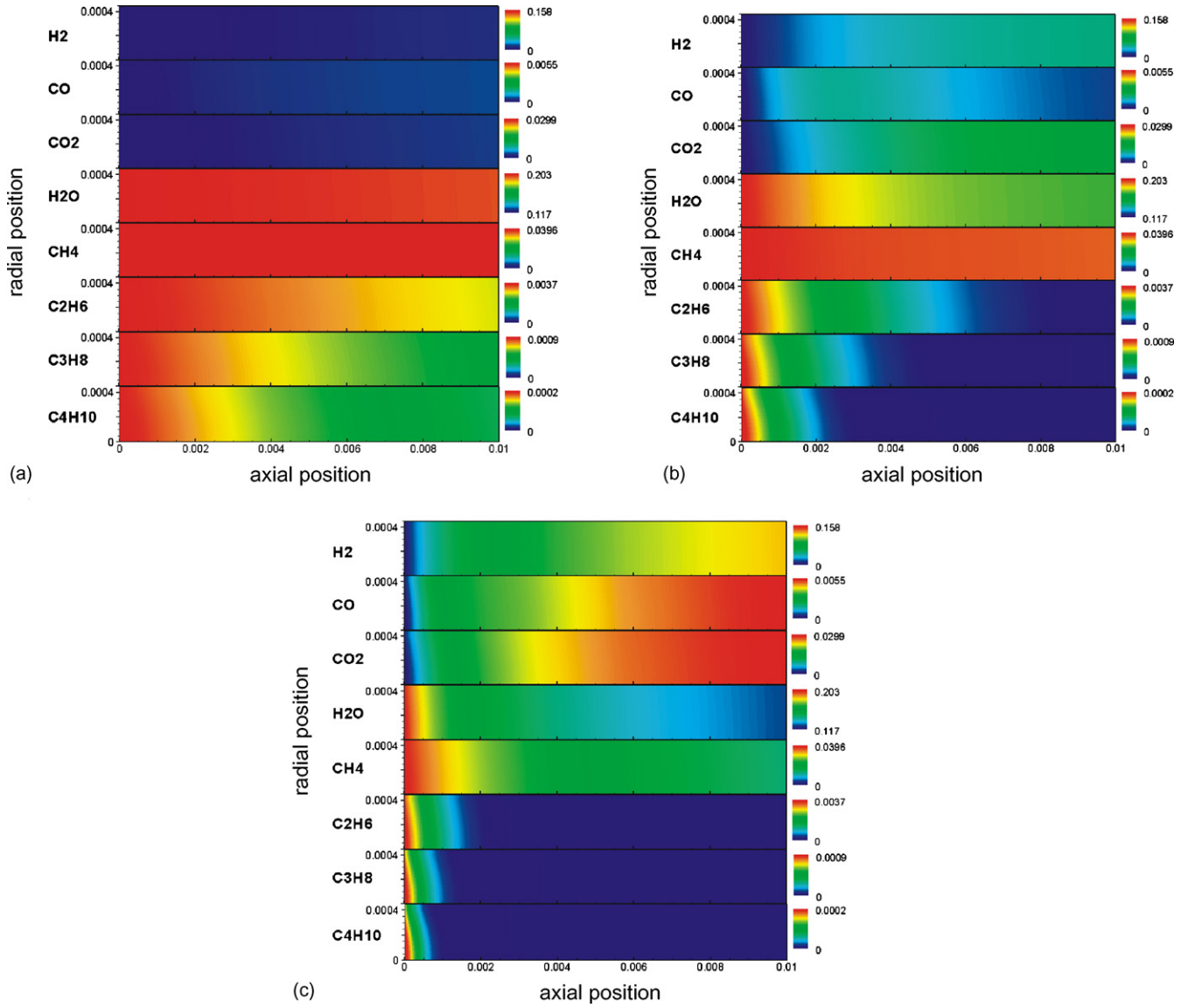


**Fig. 19.** Spatial distributions of species in the gas phase in the single channel in SR of natural gas with S/C 4 at (a) 327 °C, (b) 452 °C, (c) 577 °C; red indicates the highest and blue the lowest concentration of each species at all temperatures.

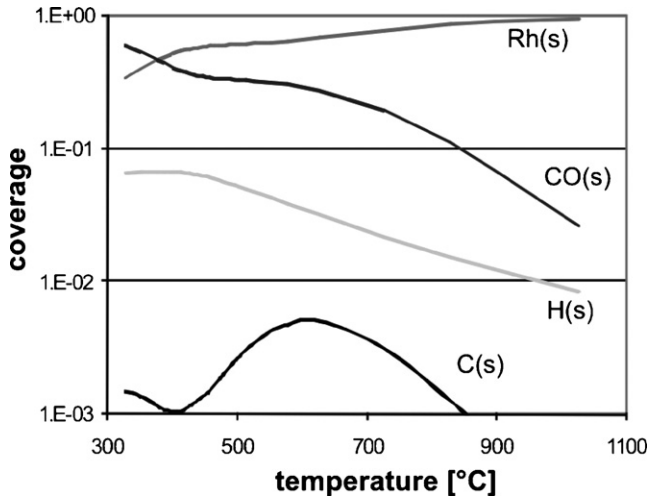


**Fig. 20.** Computed surface coverage of hydrogen, CO, and carbon in SR of natural gas with S/C 4 und 900 cpsi.

CO(s). An adsorption–desorption equilibrium cannot be reached. If, however, constant ambient conditions, temperature of 927 °C, a pressure of 1 bar and the inlet composition of SR of natural gas with S/C 4 are chosen, an equilibrium calculation using our reactions mechanism (approx. 100 s (=infinite) integration time of the kinetics) leads to a CO surface coverage of $3.5 \times 10^{-5}$. Hence, the surface coverage with adsorbed species in reactive systems can be much higher than those observed in TPD studies.

The coverage of the surface with carbon is worth mentioning: C(s) coverage reaches values up to 0.5% at 600 °C, which is also the temperature range that promotes coking as observed in aging studies.

## 7. Conclusion

Based on extensive experimental studies of SR of the major single alkane components of natural gas and SR of a sulfur-free natural gas mixture, a detailed reaction mechanism for the catalytic conversion over a Rh-based catalyst was developed and evaluated by comparison of experimentally derived and numerically predicted conversion and selectivity. The mechanism was implemented into a two-dimensional flow field description in a single monolith channel and also coupled with an elementary step reaction mechanism for potential modeling homogeneous SR in the gas phase. The mechanism can now be used to predict product distribution in SR of natural gas mixtures with varying compositions. Furthermore, the simulation tools developed allow the numerically simulation of chemical species profiles and surface coverage within catalytic monoliths.

SR of ethane, propane, and butane show almost identical conversion and selectivity as function of temperature and S/C. These dependencies are different for SR of pure methane, which, for instance, is converted as much higher temperature. The higher alkanes were found to have a positive impact on methane conversion in SR of natural gas. In the presence of a catalyst gas-phase reactions are not significant for conversion in SR of natural gas at the conditions studied.

## References

[1] J. Rostrup-Nielsen, Catalysis Today 111 (2006) 4.
[2] J.R. Rostrup-Nielsen, Catalytic steam reforming, in: J.R. Anderson, M. Boudart (Eds.), Catalysis Science and Technology, vol. 5, Springer-Verlag, New York, 1984.
[3] J.R. Rostrup-Nielsen, J. Sehested, J.K. Norskov, Advances in Catalysis 47 (2002) 65.
[4] C. Cao, Y. Wang, R.T. Rozmiarek, Catalysis Today 110 (2005) 92.
[5] S. Eriksson, S. Rojas, M. Boutonnet, J.L.G. Fierro, Applied Catalysis A: General 326 (2007) 8.
[6] E. Kikuchi, S. Tanaka, Y. Yamazaki, Y. Morita, Bulletin of the Japan Petroleum Institute 16 (1974) 95.
[7] E. Kikuchi, K. Ito, Y. Morita, Bulletin of the Japan Petroleum Institute 19 (1977) 135.
[8] S. Kurungot, T. Yamaguchi, Catalysis Letters 92 (2004) 181.
[9] Y. Mukainakano, B. Li, S. Kado, T. Miyazawa, K. Okumura, T. Miyao, S. Naito, K. Kunimori, K. Tomishige, Applied Catalysis A: General 318 (2007) 252.
[10] K. Venkataraman, E.C. Wanat, L.D. Schmidt, AIChE Journal 49 (2003) 1277.
[11] Y. Wang, Y.H. Chin, R.T. Rozmiarek, B.R. Johnson, Y. Gao, J. Watson, A.Y.L. Tonkovich, D.P. Vander Wiel, Catalysis Today 98 (2004) 575.
[12] B.I. Whittington, C.J. Jiang, D.L. Trimm, Catalysis Today 26 (1995) 41.
[13] I. Aartun, H.J. Venvik, A. Holmen, P. Pfeifer, O. Goerke, K. Schubert, Catalysis Today 110 (2005) 98.
[14] G. Kolb, R. Zapf, V. Hessel, H. Loewe, Applied Catalysis A: General 277 (2004) 155.
[15] T. Maillet, Y. Madier, R. Taha, J Barbier Jr., D. Duprez, Studies in Surface Science and Catalysis 112 (1997) 267.
[16] B. Silberova, H.J. Venvik, J.C. Walmsley, A. Holmen, Catalysis Today 100 (2005) 457.
[17] A. Igarashi, T. Ohtaka, S. Motoki, Catalysis Letters 13 (1992) 189.
[18] D. Flowers, S. Aceves, C.K. Westbrook, J.R. Smith, R. Dibble, Journal of Engineering for Gas Turbines and Power 123 (2001) 433.
[19] M. Mbarawa, B.E. Milton, R.T. Casey, International Journal of Thermal Sciences 40 (2001) 927.
[20] Z. Yu, E. Cao, Y. Wang, Z. Zhou, Z. Dai, Fuel Processing Technology 87 (2006) 695.
[21] M. Echigo, T. Tabata, Journal of Chemical Engineering of Japan 37 (2004) 723.
[22] R. Quiceno, J. Perez-Ramirez, J. Warnatz, O. Deutschmann, Applied Catalysis A: General 303 (2006) 166.
[23] D. Chatterjee, O. Deutschmann, J. Warnatz, Faraday Discussions 119 (2001) 371.
[24] D. Mantri, P. Aghalayam, Catalysis Today 119 (2007) 88.
[25] A.B. Mhadeshwar, D.G. Vlachos, Industrial & Engineering Chemistry Research 46 (2007) 5310.
[26] F. Donsi, K.A. Williams, L.D. Schmidt, Industrial & Engineering Chemistry Research 44 (2005) 3453.
[27] E.S. Hecht, G.K. Gupta, H. Zhu, A.M. Dean, R.J. Kee, L. Maier, O. Deutschmann, Applied Catalysis A: General 295 (2005) 40.
[28] V.M. Janardhanan, O. Deutschmann, Journal of Power Sources 162 (2006) 1192.
[29] A.V. Zeigarnik, R.E. Valdes-Perez, J. Pesenti, Journal of Physical Chemistry B 104 (2000) 997.
[30] Y.-Z. Lin, J. Sun, J. Yi, J.-D. Lin, H.-B. Chen, D.-W. Liao, Theochemistry 587 (2002) 63.
[31] M.J. Hei, H.B. Chen, J. Yi, Y.J. Lin, Y.Z. Lin, G. Wei, D.W. Liao, Surface Science 417 (1998) 82.
[32] O. Deutschmann, L.D. Schmidt, AIChE Journal 44 (1998) 2465.
[33] R. Schwiedernoch, S. Tischer, C. Correa, O. Deutschmann, Chemical Engineering Science 58 (2003) 633.
[34] E. ON Ruhrgas AG, technical customer service, 2007.
[35] B.T. Schädel, Untersuchung von Reformierungsprozessen von Methan an Rhodium- und Nickelkatalysatoren, diploma thesis, Fakultät für Chemie und Biowissenschaften, Universität Karlruhe (TH), 2004.
[36] L.L. Raja, R.J. Kee, O. Deutschmann, J. Warnatz, L.D. Schmidt, Catalysis Today 59 (2000) 47.
[37] O. Deutschmann, in: G. Ertl, H. Knözinger, F. Schüth, J. Weitkamp (Eds.), Handbook of Heterogeneous Catalysis, 2nd ed., Wiley–VCH, 2007 (Chapter 6.6).
[38] M.E. Coltrin, R.J. Kee, F.M. Rupley, Sandia National Laboratories, 1991
[39] I. Nakamura, Y. Kobayashi, H. Hamada, T. Fujitani, Surface Science 600 (2006) 3235.
[40] S. Tischer, C. Correa, O. Deutschmann, Catalysis Today 69 (2001) 57.
[41] O. Deutschmann, S. Tischer, S. Kleditzsch, V.M. Janardhanan, C. Correa, D. Chatterjee, N. Mladenov, H.D. Minh, DETCHEM Software Package, 2.1 ed., Karlsruhe, 2007, www.detchem.com.
[42] P. Deuflhardt, E. Hairer, J. Zugk, Numerische Mathematik 51 (1987) 501.
[43] F. Baumann, O. Deutschmann, M. Duisberg, L. Maier, L.D. Schmidt, G. Sextl, S. Wieland, in: Proceedings of the 13th International Congress on Catalysis, Paris, 2004.
[44] Q. Yan, T. Wu, L. Yang, C. Luo, W. Weng, Z. Chao, H. Wan, Journal of Natural Gas Chemistry 9 (2000) 1.
[45] E. Shustorovich, H. Sellers, Surface Science Reports 31 (1998) 1.
[46] E. Shustorovich, Advances in Catalysis 37 (1990) 101.
[47] B.T. Schädel, O. Deutschmann, in: F.B. Noronha, M. Schmal, E.F. Sousa-Aguiar (Eds.), Natural Gas Conversion VIII, Studies in Surface Science and Catalysis, vol. 167, Elsevier, Natal, 2007, p. 207.
[48] J. Wei, E. Iglesia, Journal of Catalysis 225 (2004) 116.
[49] V. Nehasil, T. Hrncir, S. Zafeiratos, S. Ladas, V. Matolin, Surface Science 454–456 (2000) 289.
[50] G. Krenn, I. Bako, R. Schennach, Journal of Chemical Physics 124 (2006) 144703–144711.